bio-protocol

Open Access

Published: Nov 20, 2025

Rapid and Solvent-Free, 2-hydroxyethyl Methacrylate (HEMA)-Acrylamide (AAm) Copolymer-Based Optical Clearing of Tissue for Fluorescent Imaging

Yanran Wang, Siying Feng, Xiaoqi Zhou, Qiufeng Yao, Hui Ma* and Kefeng Wu*

The Marine Biomedical Research Institute of Guangdong Zhanjiang, School of Ocean and Tropical Medicine, Guangdong Medical University, Zhanjiang, China
*For correspondence: mahui16@mails.ucas.ac.cn; winokhere@sina.com

Abstract

The study of whole organs or tissues and their cellular components and structures has been historically limited by their natural opacity, which is caused by the optical heterogeneity of the tissue components that scatter light as it traverses through the tissue, making 3D tissue imaging highly challenging. In recent years, tissue clearing techniques have received widespread attention and undergone rapid development. We recently demonstrated the synthesis of a 2-hydroxyethyl methacrylate (HEMA)-acrylamide (AAm) copolymer. This was achieved using antipyrine (ATP) and 2,2′-thiodiethanol (TDE) as solvents. The resulting solution rapidly embedded tissue samples with a high degree of transparency and is compatible with multiple fluorescence labeling techniques. The method exhibits significant transparency effects across a range of organs, comprising the heart, liver, spleen, lung, kidney, brain (whole and sectioned), esophagus, and small intestine. It can enable volumetric imaging of tissue up to the scale of mouse organs, decrease the duration of the clearing, and preserve emission from fluorescent proteins and dyes. To facilitate the use of this powerful tool, we have provided here a detailed step-by-step protocol that should allow any laboratory to use tissue transparency technology to achieve transparency of tissues and organs.

Key features

- The method is primarily used for optical tissue clearing.
- The method employs a HEMA-AAm copolymer for optical tissue clearing.
- This method enables both 2D and 3D fluorescence imaging.

Keywords: Copolymer, Tissue embed, Tissue clearing, Optical transparency, Fluorescence labeling, Volumetric imaging

This protocol is used in: Sci Rep (2025), DOI: 10.1038/s41598-025-94479-z

Background

There is a growing demand in the biological field for 3D volume imaging deep in biological tissues [1], but the optical heterogeneity of the tissue components results in opacity, which causes scattering of light as it penetrates the tissue [2] and makes 3D deep tissue imaging highly challenging [3]. A simple way to bypass tissue opacity is to section the thick tissue into several thin slices. Conventional tissue sectioning, however, is a laborious and time-intensive procedure and often causes tissue deformation during section preparation. Tissue-clearing techniques and high-resolution volumetric imaging by fluorescence microscopy [4,5] with appropriate fluorescent labeling can provide comprehensive cell information, such as cell type, shape, state, and distribution of cells of interest throughout an organ [6–10]. In particular, tissue-clearing techniques combined with fluorescence microscopy are a powerful tool to quantify rare cells such as stem cells, metastatic cells, or activated neurons in a whole organ for biological research and pathological diagnosis [11]. Hydrogel-based tissue clearing methods (e.g., CLARITY [12,13], PACT [14,15], SHIELD [16], SWITCH [17]) stand out for their stability and compatibility with bio-molecular staining. The intact biological tissues are replaced by a hydrogel polymerization framework, where the proteins, nucleic acids, and other macro-biomolecules are immobilized at their native physiological positions, while the lipid components remain unbound and are able to be eluted [18,19]. The decrease of the lipid barrier increases the penetrability of light and antibodies, allowing the direct stereo imaging of structural and molecular phenotyping of samples. In addition, the firm and stable hydrogel environment limits the diffusional contact between the indicator dye and reactive species, thereby improving shelf life and photochemical stability of the fluorescently labeled specimens, which is particularly important in high-resolution 3D imaging [20]. Enormous efforts have been made to fabricate hydrogels with enhanced mechanical properties by using hybrid hydrogels [21,22] or nano-composite hydrogels or by designing distinctive structures such as an interpenetrating network and dual-crosslinking network. By adjusting the hydrogel's composition, the chemical environment of the tissue-hydrogel complex can be engineered to create a favorable condition for tissue clearing [23].

The 2-hydroxyethyl methacrylate-acrylamide (HEMA-Aam) method significantly outperformed most hydrogel-based clearing techniques, particularly in terms of clearing speed, tissue transparency, and size preservation. This approach effectively preserves tissue morphology and is compatible with fluorescence labeling, making it optimal for high-resolution imaging and long-term studies. The HEMA-AAm method achieved a high level of transparency in centimeter-scale mouse kidneys within four days. In comparison, the PACT method achieved similar transparency in approximately six days, while the TESOS method required several weeks. However, the TESOS method, despite offering relatively good transparency, exhibited high toxicity and caused severe fluorescence quenching. The PACT method displayed the poorest overall performance and lacked practical utility. During the process, we observed an increase in kidney tissue size from 100% (PBS) to 110% ± 2%, indicating negligible tissue expansion to maintain the size of the samples caused by the immersion and embedding processes. In contrast, the TESOS and PACT methods induced significant expansion or contraction of the samples. This transparent and hydrogel condition provides a friendly tissue and cellular environment to facilitate high-resolution 3D imaging, preservation, transfer, and sharing among laboratories to investigate the morphologies of interest in experimental and clinical conditions. Here, we offer a comprehensive and progressive process to facilitate the transparent handling of tissues and organs. We also describe how to handle tissue samples, including the preparation of immunofluorescence staining and the preparation of hydrogels.

Materials and reagents

Biological materials

1. 8–12-week-old wild-type C57BL/6 mice (Guangdong Laboratory Animal Monitoring Institute)
2. Enhanced green fluorescent protein (EGFP) transgenic mice (Jiangsu Huachuang Xinnuo Medical Technology Co, Ltd.)

Reagents

1. Antipyrine (ATP) (Shanghai Macklin Biochemical Co, Ltd, catalog number: 60-80-0)
2. Acrylamide (AAm) (Shanghai Macklin Biochemical Co, Ltd, catalog number: 79-06-1)
3. Poly(ethylene glycol) diacrylate (PEGDA) (Shanghai Macklin Biochemical Co, Ltd, catalog number: 25736-86-1)

4. 2,2'-Azobis[2-(2-imidazolin-2-yl)propane] dihydrochloride (VA-044) (Shanghai Macklin Biochemical Co, Ltd, catalog number: 27776-21-2)
5. Thiodiglycol (TDE) (Kryptonite Ltd, catalog number: CD101467)
6. 2-Hydroxyethyl methacrylate (2-HEMA) (Aladdin, catalog number: 868-77-9)
7. 4% paraformaldehyde (PFA) (Leagene, catalog number: DF0135)
8. 0.02% sodium azide (Aladdin, catalog number: 26628-22-8)
9. 2% Triton X-100 (Aladdin, catalog number: 9036-19-5)
10. CD31 antibody [Signalway Antibody (SAB), RRID: AB_852501]
11. Perilipin A Rabbit mAb [Signalway Antibody (SAB), RRID: AB_2863342]
12. Goat anti-rabbit lgG secondary antibody AF488 conjugated (Jackson ImmunoResearch, RRID: AB_3246434)
13. Lectin (Vector Labs, RRID: AB_2314736)
14. DAPI (Sigma-Aldrich, RRID: AB_2869624)
15. PBS (Servicebio, catalog number: G0002)
16. Isoflurane (Nanjing Aibei Biotechnology Co, Ltd, catalog number: 2409A)
17. Primary antibody dilution buffer, QuickBlock™ immunostaining primary antibody dilution buffer (Beyotime, catalog number: P0262)
18. Secondary antibody dilution buffer, QuickBlock™ immunostaining secondary antibody dilution buffer (Beyotime, catalog number: P0265)
19. Blocking buffer, QuickBlock™ immunostaining blocking buffer (Beyotime, catalog number: P0260)

Solutions

1. Tissue clearing solution (see Recipes)
2. Monomer solution (see Recipes)
3. Prepolymer solution (see Recipes)
4. 0.01 M PBS (see Recipes)

Recipes

1. Tissue clearing solution

Reagent	Final concentration	Quantity or Volume
ATP	348 g/L	1.8823 g
TDE	450 g/L	2.062 mL
Distilled water	216 g/L	1.0815 mL
Total	998 g/L	~5.4 mL

2. Monomer solution

Reagent	Final concentration	Quantity or volume
AAm	-	0.3 g
2-HEMA	0.1 mL	1.82 mL
PEGDA	0.1 mL	0.155 mL
Total	-	-

Critical: 2-HEMA and PEGDA solutions are first mixed together, and then 1 mL of the mixture is taken and added to the subsequent prepolymer solution.

3. Prepolymer solution

Reagent	Final concentration	Quantity or volume
Monomer solution	404.9 g/L	0.3 g + 0.1 mL
Tissue clearing solution	1,062 g/L	0.9 mL
Total	1,466.9 g/L	~1.0 mL

Critical: Following preparation of the prepolymer solution, a 1 mL aliquot is mixed with 15 µL of VA-044 to induce gel formation through polymerization.

4. 0.01 M PBS

Reagent	Final concentration	Quantity or volume
PBS powder	0.01 M	One sachet (commercially provided)
Distilled water	-	2 L
Total	-	2 L

Note: The PBS solution was prepared by dissolving commercially obtained PBS powder in 2 L of deionized water.

Laboratory supplies

1. 1,000 µL pipette tips (BioSharp, catalog number: 24824031E)
2. 1,000 µL pipette (Thermo Fisher, catalog number: MZ11332)
3. 100 µL pipette tips (BioSharp, catalog number: 21223639E)
4. 100 µL pipette (Thermo Fisher, catalog number: QZ55048)
5. 20 µL pipette (Thermo Fisher, catalog number: TO19723)
6. 24 × 24 mm standard-grade microscope coverslips (Citotest, catalog number: 10212424C)
7. 7 × 7 × 5 mm embedding cassette base mold (Citotest, catalog number: 80203-0006)
8. 15 mL centrifuge tube (BioSharp, catalog number: 30324124E)
9. 50 mL centrifuge tube (BioSharp, catalog number: 35224125E)
10. 5.0 mL microcentrifuge tube (BioSharp, catalog number: 23029335A)
11. 2.0 mL microcentrifuge tube (BioSharp, catalog number: 241211)
12. Adhesive (Pattex, catalog number: 24032809)
13. Pasteur pipette (Kangpeite, catalog number: 20240136)
14. 30 mL sterile syringe (Hongda, catalog number: 20193141735)
15. 1 mL sterile syringe (Hongda, catalog number: 20193141735)
16. Disposable intravenous infusion needle (Hongda, catalog number: 20173144093)
17. Cryostat [Dakewe (Shenzhen) Medical Equipment Co., Ltd., model CT520]

Equipment

1. Light-sheet fluorescence microscope (Nuohai, model: LS18)
2. Digital ultrasonic cleaner (Kangshijie, model: PL-S40T)
3. Air-bath thermostatic shaker (Jinyi, model: THZ-82B, serial number: XMTD-702)
4. Confocal microscope (Olympus, model: IXplore spinSR)
5. Horizontal rotator (Taizhou Nuomi Medical Technology Co, Ltd, model: NMYC-100)
6. Automatic refractometer (Shanghai Yimai Instrument Technology Co, Ltd, model: IR140)
7. Cryostat stage (MEDITE Medical, Leica CM1950)

Software and datasets

The data in the figure and legend of the manuscript are presented as mean ± standard deviation (x ± s). Statistical analysis was conducted using t-tests or one-way analysis of variance (ANOVA) as appropriate. Statistical analyses were performed using ImageJ, GraphPad Prism and origin, 3D reconstruction was performed using AIVIA (version 14, Manufacturer Information:Leica Microsystems (Shanghai) Trading Co., Ltd.). All data and analysis needed for the development and characterization of this protocol are available in the main text or Supplemental Information of Qin et al. [24].

Procedure

A. Animal tissue sample preparation

Notes:
1. Harvested tissues were fixed in 4% PFA at 4 °C.
2. The vasculature was labeled via cardiac perfusion using DyLight 594-conjugated Lycopersicon esculentum *(Tomato) lectin (LEL-DyLight 594, Vector Laboratories).*

1. Mice were fasted for a period of 24 h prior to tissue collection to minimize interference from food residues in subsequent experiments. Lectin was diluted with PBS at a ratio of 1:1,000, yielding a total volume of 15 mL. To facilitate cardiac perfusion, the mouse was initially anesthetized using an appropriate dose of isoflurane. An abdominal incision was then made to expose the heart, followed by a small incision at the upper left corner of the heart to drain the blood. The anesthetized mouse was subsequently perfused with 0.01 M PBS at a rate of 1–2 mL/min. This was succeeded by perfusion with 10–15 mL of the lectin solution, maintaining the same rate. The mouse was ultimately fixed by perfusion with 4% PFA.
Note: The perfusion speed should not be too fast when using PBS or PFA.
2. Dissect out the mouse and tissues (including but not limited to the heart, liver, spleen, lung, kidney, brain, esophagus, and small intestine). Immerse them in PBS solution. After tissue collection is completed, place the harvested tissues in 4% PFA for overnight fixation at 4 °C.
Note: Tissues must be fixed in 4% PFA for at least 12 h.
3. Store the tissues in PBS containing 0.02% sodium azide at 4 °C for further processing.

B. Immunostaining

Notes:
1. Keep the labeled antibodies in the dark.
2. Rinse the samples thoroughly with PBS every time when switching antibodies.

1. After retrieving the target tissues from the 4 °C refrigerator, rinse them three times with 5 mL of PBS on a shaker at 37 °C and 50 rpm, allowing at least 1 h per wash.
2. Incubate the tissues in 2% Triton X-100 solution at 37 °C for 24 h, followed by overnight blocking with blocking buffer at 37 °C.
3. Rinse the tissues three times with PBS (minimum 1 h per wash), then prepare the primary antibody at the desired concentration (1:50) using antibody diluent, and incubate at 37 °C with 50 rpm shaking for 48 h. Dilute the secondary antibody 1:100 in antibody diluent and apply it to samples at 37 °C with 50 rpm agitation for 24 h. After incubation, remove excess antibody by three PBS washes (≥1 h each) under the same conditions.
4. Perform nuclear staining by incubating with DAPI at 37 °C for 12 h.
Note: When the research involves intact and un-sectioned mouse organs (such as whole brain, kidney, and small intestine), which are quite thick, a prolonged incubation time is necessary to allow enough time for DAPI to adequately penetrate and diffuse to the nuclei of cells located deep within the tissue. In contrast, a short incubation time is sufficient for sectioned tissues. The specific incubation time can be adjusted according to the actual experimental conditions, and a 12-h DAPI incubation time was used in this study, ensuring the optimal DAPI staining signal was obtained.
5. Following antibody/dye labeling, wash tissues three times in PBS (1 h each) before tissue clearing processing.
Note: Repeat the aforementioned steps sequentially for any additional antibody staining.

C. HEMA-AAm copolymer production

Notes:
1. The thiodiglycol used in this copolymer synthesis is now prohibited for domestic purchase in China, though it remains available internationally. Our laboratory's stock was acquired prior to the implementation of these restrictions.
2. Due to thiodiglycol's volatile and irritating nature, all experiments were performed in a certified chemical fume hood.
3. Maintain experimental humidity below 60% RH.
4. Gel formation was carried out at 37–50 °C for 6–36 h under controlled conditions.

5. Optimal results were obtained with the antipyrine-thiodiglycol solution at water concentrations between 20% and 25% (w/w).
6. The tissue optical clearing solution was prepared using the mixed solution at 20%–25% water content, while the prepolymerization solution for subsequent reactions contained precisely 20% water.

1. Synthesize HEMA-AAm copolymer via free radical polymerization. Prepare tissue optical clearing solution following Recipe 1 (e.g., 1.88 g ATP + 2.06 mL TDE + 1.08 mL H_2O), followed by heating at 40 °C for 4 h with agitation.
2. The copolymerization system consists of AAm and HEMA as co-monomers, with PEGDA (Mn = 700) as the crosslinking agent and VA-044 as the thermal initiator.
3. Thoroughly mix PEGDA (0.155 mL) with 2-HEMA (1.82 mL).

Critical:$n_{2\text{-HEMA}}$:n_{pegda} = 15:1

4. Prepare prepolymer solution by adding 0.9 mL of the ATP/TDE/water mixture (1:2 ratio, see step C1) and 0.3 g of AAm to 0.1 mL of the PEGDA/2-HEMA blend, followed by homogenization at 45 °C.
5. Next, transfer 1 mL of the prepared prepolymer solution into a reaction vial, add 15 µL of VA-044 initiator, and incubate at 37 °C for 12 h to form the copolymer gel.
Critical: The VA-044 initiator was prepared by dissolving 0.1 g of 2,2'-azobis[2-(2-imidazolin-2-yl)propane] dihydrochloride in 1 mL of water. The remaining VA-044 solution can be stored at 4 °C, although it is recommended not to exceed two weeks of storage.
6. In summary, a tough, high-refractive-index copolymer was synthesized via free-radical copolymerization of AAm and HEMA monomers in ATP/TDE solvent with PEGDA as crosslinker, as illustrated in Figure 1.

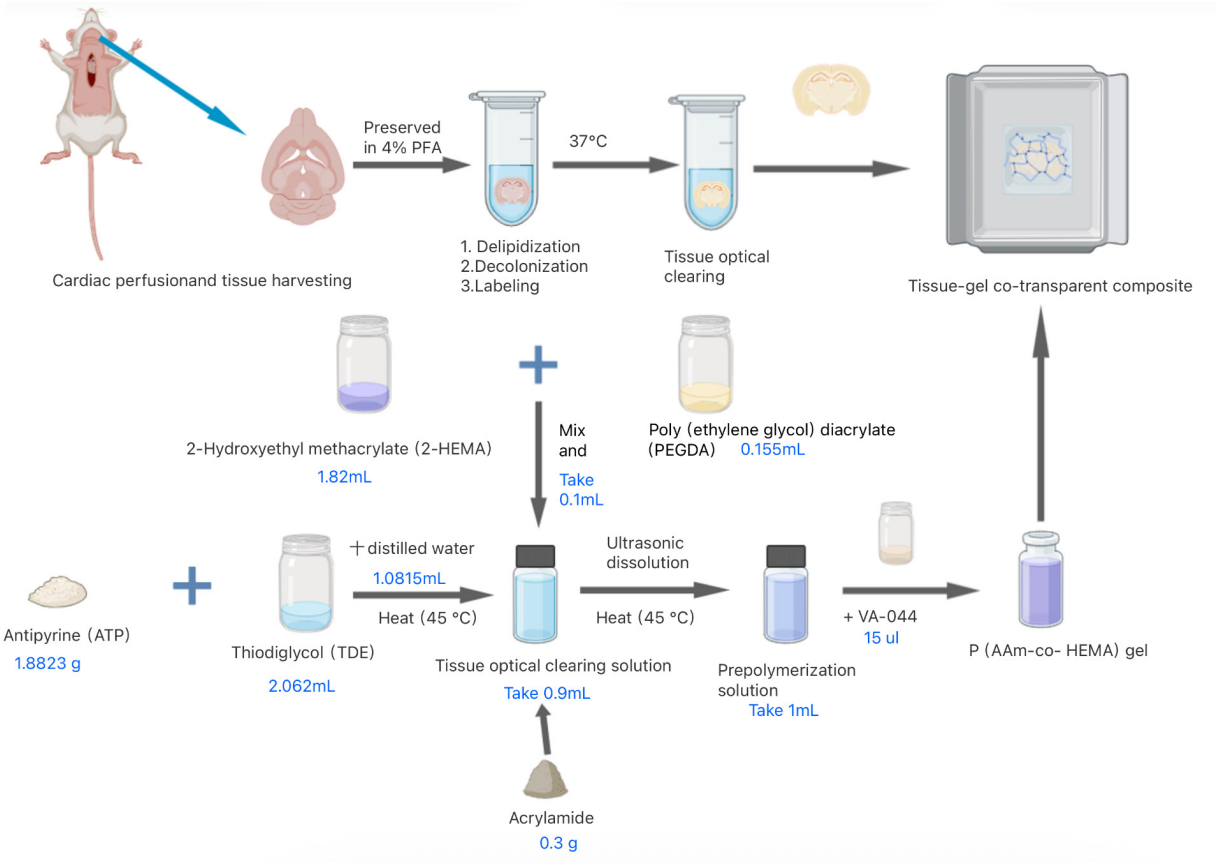

Figure 1. Preparation process of HEMA-AAm copolymer for optical clearance

D. Optical tissue clearing method

Notes:
1. The optimal relative humidity for the experiments was determined to be 60% RH.
2. The clearing agent formulation permits water content between 20%–25% (w/w), corresponding to 20%–25% aqueous component in the antipyrine/thiodiglycol mixture.

1. Wash the 4% PFA-fixed tissues 3 times with PBS (1 h per wash), then perform immunofluorescence staining followed by optical tissue clearing (steps are as shown in B).
2. Immerse the stained tissue in tissue clearing solution at 37 °C for 24 h to achieve tissue transparency.
3. Prepare fresh monomer solution, mix with VA-044 initiator (15 μL per 1 mL), and cast into embedding molds (7 × 7 × 5 mm). Immerse tissues in the solution and polymerize at 37 °C for 24 h to enable refractive index matching.
4. To demonstrate the hydrogel's performance in organ/tissue imaging, Figure 2 presents the clearing outcomes of various organs/tissues (e.g., heart, liver, spleen, lung, kidney, brain, esophagus, and small intestine; n = 3) using the HEMA-AAm copolymer. All tissues achieved high transparency, though the final transparency levels of the tissue-gel co-clearing composites varied.

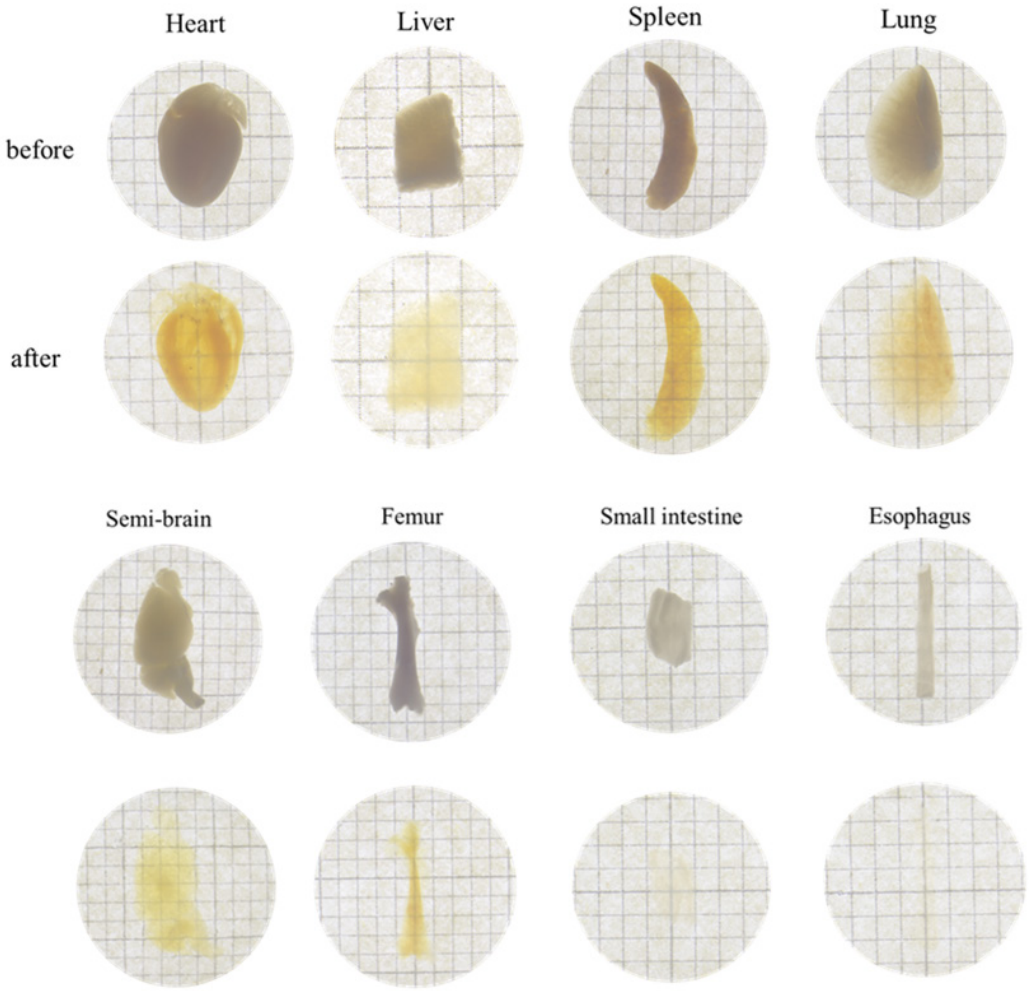

Figure 2. Optical clearing of various tissues using HEMA-AAm copolymer before and after tissue clearing

E. Tissue-gel co-clearing cryosections

Note: Cryosectioning was performed following 3D imaging, with the sections used for 2D imaging.
1. After 3D imaging, retrieve the co-cleared tissue gel from the imaging solution, embed it in OCT compound, and place it on the cryostat stage until solidified and securely adhered to the sample holder.
2. Adjust the cryostat temperature to between -20 and -25 °C, then secure the frozen tissue-gel block on the microtome.
3. Subsequently, section the block into 30–50 μm thick slices and mount them on glass slides for microscopic examination.
4. By combining conventional cryosectioning techniques, we achieved direct sectioning of tissue-gel co-cleared composites at 30–50 μm thickness for subsequent 2D imaging via super-resolution confocal microscopy. Figure 3 demonstrates 2D fluorescence images of immunolabeled, gel-embedded small intestinal sections, revealing distinct $CD31^+$ vascular endothelium and DAPI-stained nuclear architectures. The sections exhibited high fluorescence retention with minimal quenching.

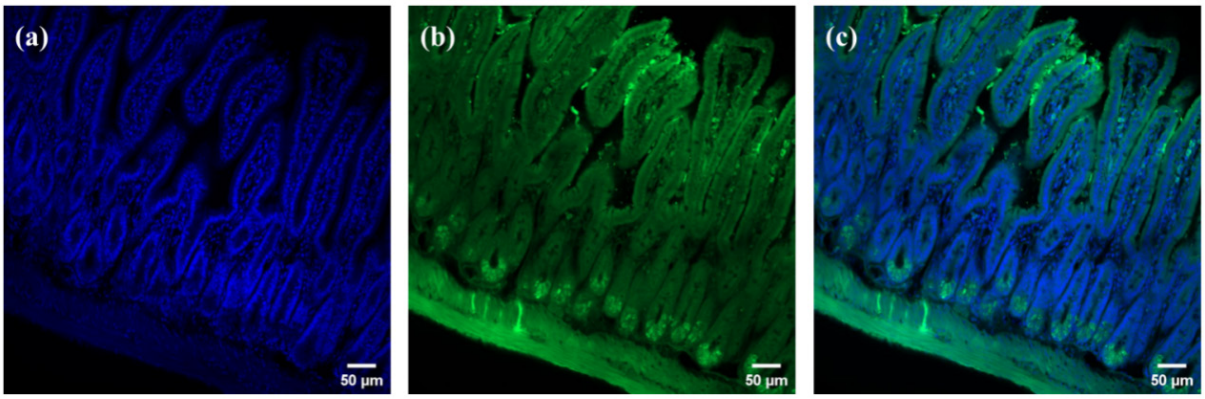

Figure 3. 3D-to-2D retrospective analysis of immunofluorescence imaging. Small intestinal sections labeled with (a) DAPI, (b) CD31, and (c) merged CD31 and DAPI signals.

F. Fluorescence imaging

Notes:
1. Mouse tissues were immobilized in 2-HEMA/AAm copolymer hydrogels, generating refractive-index-matched tissue-gel hybrids suitable for high-resolution 3D imaging.
2. Use the cryosectioned tissues for 2D imaging.

1. Perform fluorescence imaging using a light-sheet microscope (Nuohai LS18) for 3D imaging of cleared tissues to visualize immunostaining and EGFP signals.
2. Use the confocal microscope to provide high-resolution 2D fluorescence images.
3. Employ light sheet fluorescence microscopy (LSFM) to enable 3D volumetric imaging of intact tissue architecture with preserved signal integrity.
4. Acquire Figure 4A, which displays a 3D reconstruction of intestinal tissue, by confocal laser scanning microscopy (CLSM).
5. Obtain Figure 4B, which shows higher-resolution CLSM imaging, from the same specimen.
6. Acquire Figure 4C, a 3D image of intestinal tissue, by light-sheet fluorescence microscopy (LSFM).
7. Use hydrogel-based tissue clearing to prepare the mouse intestine sample.
8. Apply LSFM to clearly resolve DAPI-stained nuclear structures and lectin-labeled vasculature throughout the entire cleared mouse intestine.
9. Immunofluorescently label the mouse intestinal sections.
10. Process the labeled sections with a copolymer hydrogel.
11. Display the 3D reconstruction of a detailed vascular tree network in Figure 4D.
12. Use intact lung lobes from EGFP mice to demonstrate whole-organ imaging.
13. Process the lung lobes through complete tissue clearing.
14. Perform volumetric imaging on the cleared lung lobes.

15. Use the 3D bright fluorescence image in Figure 5 to reveal the morphology of both tracheal structures and venous networks.

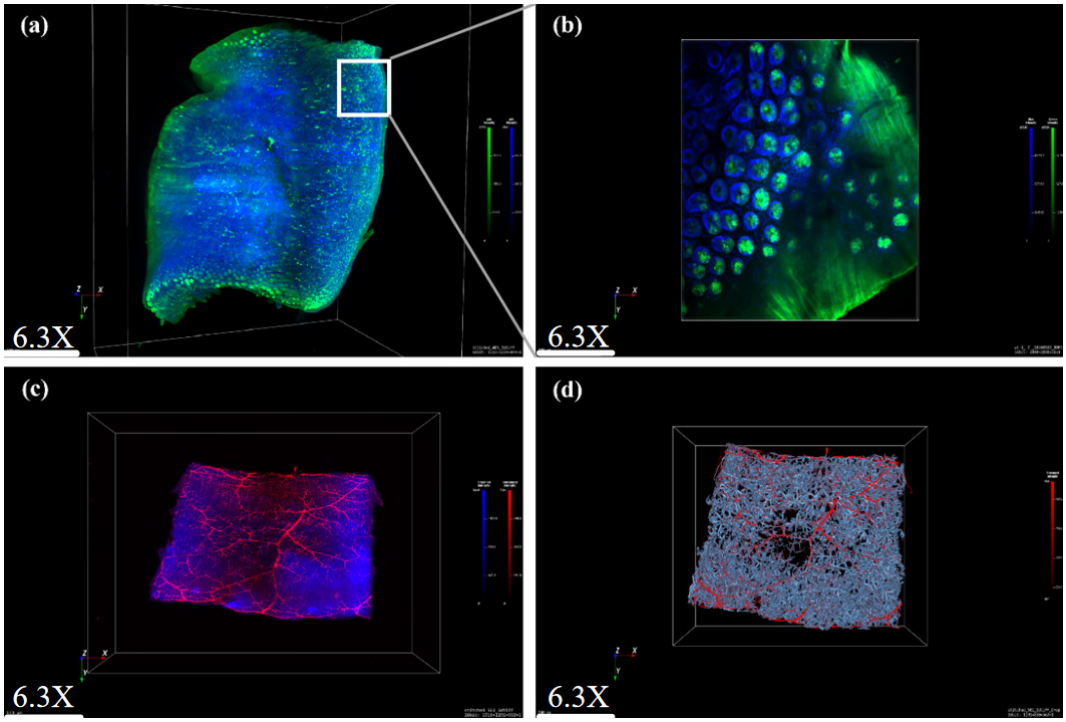

Figure 4. 3D visualization of CD31 and DAPI-labeled small intestine. (A) 6.3× magnification, light-sheet fluorescence microscopy (LSFM). (B) 10× magnification, confocal laser scanning microscopy (CLSM). (C) Lectin and DAPI labeling, 6.3×, LSFM. (D) 3D reconstruction of intestinal vascular network using AIVIA software.

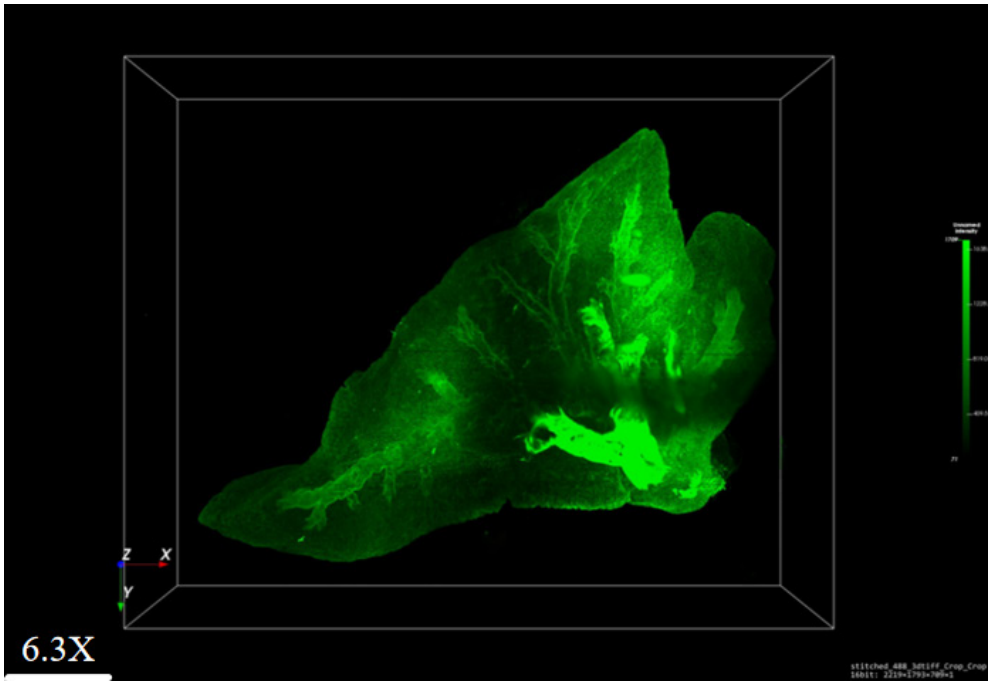

Figure 5. 3D visualization of lung lobes from EGFP fluorescent mice

Validation of protocol

This protocol (or parts of it) has been used and validated in the following research article(s):
• Ma et al. [24]. Application of HEMA-AAm copolymer to achieve faster optical tissue transparency for 2D/3D fluorescence imaging. *Sci Rep.* 15(1): e1038/s41598–025–94479–z. https://doi.org/10.1038/s41598-025-94479-z

General notes and troubleshooting

Troubleshooting

Problem 1: The liquid failed to polymerize into a gel.
Possible causes: (1) Expired VA-044 initiator. (2) Ambient humidity exceeding acceptable limits. (3) Reagent expiration.
Solutions: (1) Maintain humidity at ≤60% RH. (2) Use only non-expired reagents. (3) Employ freshly opened VA-044.

Acknowledgments

This work was supported by the Fund of Southern Marine Science and Engineering Guangdong Laboratory (Zhanjiang) (ZJW-2019-007), the Special Funds for Economic Development of Marine Economy of Guangdong Province, China (GDME-2018C011), the Special Science and Technology Innovation Project of Guangdong Province, China (2019A01005, 2019A03023), Natural Science Foundation of Shandong Province (ZR2023QB205) and (ZR2022MB027), and Youth Research Projects of Guangdong Medical University (GDMUD2024005). This protocol was used in [24].

Author Contributions:
Yanran Wang: Formal analysis and Original Draft, Siying Feng: Investigation and Data Curation, Xiaoqi Zhou: Visualization and Validation, Qiufeng Yao: Software and Supervision, Hui Ma: Review & Editing and Kefeng Wu: Funding acquisition.

Competing interests

The authors declare no competing interests.

Ethical considerations

All animal procedures were conducted in accordance with the National Research Council's Guide for the Care and Use of Laboratory Animals Science, which complied with the ARRIVE guidelines (https://arriveguidelines.org/) and U.S. National Institutes of Health (NIH) Guide for the Care and Use of Laboratory Animals. All experiments were approved by the Institutional Animal Care and Use Committee (IACUC) of the Guangdong Laboratory Animals Monitoring Institute (Guangzhou, China, NO. A-IACUC2023104).

Received: July 30, 2025; Accepted: September 19, 2025; Available online: October 17, 2025; Published: November 20, 2025

References

1. Mofazzal Jahromi, M. A., Sahandi Zangabad, P., Moosavi Basri, S. M., Sahandi Zangabad, K., Ghamarypour, A., Aref, A. R., Karimi, M. and Hamblin, M. R. (2018). Nanomedicine and advanced technologies for burns: Preventing infection and facilitating wound healing. *Adv Drug Delivery Rev.* 123: 33–64. https://doi.org/10.1016/j.addr.2017.08.001
2. Ni, Y., Wu, J., Liu, F., Yi, Y., Meng, X., Gao, X., Xiao, L., Zhou, W., Chen, Z., Chu, P., et al. (2025). Deep imaging of LepR+ stromal cells in optically cleared murine bone hemisections. *Bone Res.* 13(1): e1038/s41413–024–00387–9. https://doi.org/10.1038/s41413-024-00387-9
3. Kim, K., Na, M., Oh, K., Cho, E., Han, S. S. and Chang, S. (2022). Optimized single-step optical clearing solution for 3D volume imaging of biological structures. *Commun Biol.* 5(1): e1038/s42003–022–03388–8. https://doi.org/10.1038/s42003-022-03388-8
4. Dodt, H. U., Leischner, U., Schierloh, A., Jährling, N., Mauch, C. P., Deininger, K., Deussing, J. M., Eder, M., Zieglgänsberger, W., Becker, K., et al. (2007). Ultramicroscopy: three-dimensional visualization of neuronal networks in the whole mouse brain. *Nat Methods.* 4(4): 331–336. https://doi.org/10.1038/nmeth1036
5. Rousselle, P., Braye, F. and Dayan, G. (2019). Re-epithelialization of adult skin wounds: Cellular mechanisms and therapeutic strategies. *Adv Drug Delivery Rev.* 146: 344–365. https://doi.org/10.1016/j.addr.2018.06.019
6. Glaser, A. K., Reder, N. P., Chen, Y., McCarty, E. F., Yin, C., Wei, L., Wang, Y., True, L. D. and Liu, J. T. C. (2017). Light-sheet microscopy for slide-free non-destructive pathology of large clinical specimens. *Nat Biomed Eng.* 1(7): e1038/s41551–017–0084. https://doi.org/10.1038/s41551-017-0084
7. Kim, Y., Venkataraju, K. U., Pradhan, K., Mende, C., Taranda, J., Turaga, S. C., Arganda-Carreras, I., Ng, L., Hawrylycz, M. J., Rockland, K. S., et al. (2015). Mapping Social Behavior-Induced Brain Activation at Cellular Resolution in the Mouse. *Cell Rep.* 10(2): 292–305. https://doi.org/10.1016/j.celrep.2014.12.014
8. Kubota, S. I., Takahashi, K., Nishida, J., Morishita, Y., Ehata, S., Tainaka, K., Miyazono, K. and Ueda, H. R. (2017). Whole-Body Profiling of Cancer Metastasis with Single-Cell Resolution. *Cell Rep.* 20(1): 236–250. https://doi.org/10.1016/j.celrep.2017.06.010
9. Nojima, S., Susaki, E. A., Yoshida, K., Takemoto, H., Tsujimura, N., Iijima, S., Takachi, K., Nakahara, Y., Tahara, S., Ohshima, K., et al. (2017). CUBIC pathology: three-dimensional imaging for pathological diagnosis. *Sci Rep.* 7(1): 9269. https://doi.org/10.1038/s41598-017-09117-0
10. Tomer, R., Lovett-Barron, M., Kauvar, I., Andalman, A., Burns, V. M., Sankaran, S., Grosenick, L., Broxton, M., Yang, S., Deisseroth, K., et al. (2015). SPED Light Sheet Microscopy: Fast Mapping of Biological System Structure and Function. *Cell.* 163(7): 1796–1806. https://doi.org/10.1016/j.cell.2015.11.061
11. Murakami, T. C., Mano, T., Saikawa, S., Horiguchi, S. A., Shigeta, D., Baba, K., Sekiya, H., Shimizu, Y., Tanaka, K. F., Kiyonari, H., et al. (2018). A three-dimensional single-cell-resolution whole-brain atlas using CUBIC-X expansion microscopy and tissue clearing. *Nat Neurosci.* 21(4): 625–637. https://doi.org/10.1038/s41593-018-0109-1
12. Chung, K. and Deisseroth, K. (2013). CLARITY for mapping the nervous system. *Nat Methods.* 10(6): 508–513. https://doi.org/10.1038/nmeth.2481
13. Jensen, K. H. R. and Berg, R. W. (2017). Advances and perspectives in tissue clearing using CLARITY. *J Chem Neuroanat.* 86: 19–34. https://doi.org/10.1016/j.jchemneu.2017.07.005
14. Treweek, J. B., Chan, K. Y., Flytzanis, N. C., Yang, B., Deverman, B. E., Greenbaum, A., Lignell, A., Xiao, C., Cai, L., Ladinsky, M. S., et al. (2015). Whole-body tissue stabilization and selective extractions via tissue-hydrogel hybrids for high-resolution intact circuit mapping and phenotyping. *Nat Protoc.* 10(11): 1860–1896. https://doi.org/10.1038/nprot.2015.122
15. Yang, B., Treweek, J. B., Kulkarni, R. P., Deverman, B. E., Chen, C. K., Lubeck, E., Shah, S., Cai, L. and Gradinaru, V. (2014). Single-Cell Phenotyping within Transparent Intact Tissue through Whole-Body Clearing. *Cell.* 158(4): 945–958. https://doi.org/10.1016/j.cell.2014.07.017
16. Park, Y. G., Sohn, C. H., Chen, R., McCue, M., Yun, D. H., Drummond, G. T., Ku, T., Evans, N. B., Oak, H. C., Trieu, W., et al. (2019). Protection of tissue physicochemical properties using polyfunctional crosslinkers. *Nat Biotechnol.* 37(1): 73–83. https://doi.org/10.1038/nbt.4281
17. Murray, E., Cho, J. H., Goodwin, D., Ku, T., Swaney, J., Kim, S. Y., Choi, H., Park, Y. G., Park, J. Y., Hubbert, A., et al. (2015). Simple, Scalable Proteomic Imaging for High-Dimensional Profiling of Intact Systems. *Cell.* 163(6): 1500–1514. https://doi.org/10.1016/j.cell.2015.11.025
18. Borchers, A. and Pieler, T. (2010). Programming Pluripotent Precursor Cells Derived from Xenopus Embryos to Generate Specific Tissues and Organs. *Genes (Basel).* 1(3): 413–426. https://doi.org/10.3390/genes1030413

19. Hsiao, F. T., Chien, H. J., Chou, Y. H., Peng, S. J., Chung, M. H., Huang, T. H., Lo, L. W., Shen, C. N., Chang, H. P., Lee, C. Y., et al. (2023). Transparent tissue in solid state for solvent-free and antifade 3D imaging. *Nat Commun.* 14(1): e1038/s41467–023–39082–4. https://doi.org/10.1038/s41467-023-39082-4
20. Kojima, C., Koda, T., Nariai, T., Ichihara, J., Sugiura, K. and Matsumoto, A. (2021). Application of Zwitterionic Polymer Hydrogels to Optical Tissue Clearing for 3D Fluorescence Imaging. *Macromol Biosci.* 21(9): e202100170. https://doi.org/10.1002/mabi.202100170
21. Dohi, S., Suzuki, Y. and Matsumoto, A. (2020). One-shot radical polymerization of vinyl monomers with different reactivity accompanying spontaneous delay of polymerization for the synthesis of double-network hydrogels. *Polym Int.* 69(10): 954–963. https://doi.org/10.1002/pi.6048
22. Li, J., Chee, H. L., Chong, Y. T., Chan, B. Q. Y., Xue, K., Lim, P. C., Loh, X. J. and Wang, F. (2022). Hofmeister Effect Mediated Strong PHEMA-Gelatin Hydrogel Actuator. *ACS Appl Mater Interfaces.* 14(20): 23826–23838. https://doi.org/10.1021/acsami.2c01922
23. Ono, Y., Nakase, I., Matsumoto, A. and Kojima, C. (2019). Rapid optical tissue clearing using poly(acrylamide-co-styrenesulfonate) hydrogels for three-dimensional imaging. *J Biomed Mater Res Part B Appl Biomater.* 107(7): 2297–2304. https://doi.org/10.1002/jbm.b.34322
24. Ma, H., Qin, R., Yao, Q., Li, Y., Cong, X., Wu, W., Zhao, Q., Ye, H. and Wu, K. (2025). Application of HEMA-AAm copolymer to achieve faster optical tissue transparency for 2D/3D fluorescence imaging. *Sci Rep.* 15(1): e1038/s41598–025–94479–z. https://doi.org/10.1038/s41598-025-94479-z